



HAL
open science

Design optimization of a 2D blade by means of milling tool path

Christian Vessaz, Christophe Tournier, Cécile Munch, François Avellan

► **To cite this version:**

Christian Vessaz, Christophe Tournier, Cécile Munch, François Avellan. Design optimization of a 2D blade by means of milling tool path. CIRP Journal of Manufacturing Science and Technology, 2013, 6, pp.157-166. 10.1016/j.cirpj.2013.05.002 . hal-00843631

HAL Id: hal-00843631

<https://hal.science/hal-00843631>

Submitted on 12 Jul 2013

HAL is a multi-disciplinary open access archive for the deposit and dissemination of scientific research documents, whether they are published or not. The documents may come from teaching and research institutions in France or abroad, or from public or private research centers.

L'archive ouverte pluridisciplinaire **HAL**, est destinée au dépôt et à la diffusion de documents scientifiques de niveau recherche, publiés ou non, émanant des établissements d'enseignement et de recherche français ou étrangers, des laboratoires publics ou privés.

Design optimization of a 2D blade by means of milling tool path

Christian Vessaz^a, Christophe Tournier^{b,*}, Cécile Münch^c, François Avellan^a

^a*EPFL, École polytechnique fédérale de Lausanne, Laboratory for Hydraulic Machines, avenue de Cour 33 bis, 1007 Lausanne, Switzerland*

^b*LURPA, ENS Cachan, Université Paris Sud 11, 61 avenue du Président Wilson, 94235 Cachan, France*

^c*HES SO Valais, Haute école spécialisée de Suisse occidentale, Institut Systèmes industriels, Route du Rawyl 47, 1950 Sion, Switzerland*

Abstract

In a conventional design and manufacturing process, turbine blades are modeled based on reverse engineering or on parametric modeling with Computer Fluids Dynamics (CFD) optimization. Then, only raises the question of the manufacturing of the blades. As the design does not take into account machining constraints and especially tool path computation issues in flank milling, the actual performance of the machined blade could not be optimal. In this paper, a new approach is used for the design and manufacture of turbine blades in order to ensure that the simulated machined surface produces the expected hydraulic properties. This consists in the modeling of a continuous tool path based on numerical simulation rather than the blade surface itself. Consequently, this paper aims at defining the steps of the proposed design approach including geometrical modeling, mesh generation, CFD simulation and genetic optimization. The method is applied on an isolated blade profile in a uniform water flow and results are compared to the conventional design process.

Keywords: Design for manufacturing, Tool path, Flank milling, Genetic optimization, Blades

*Corresponding author Tel.: +33 1 47 40 29 96; Fax: +33 1 47 40 22 11
Email address: christophe.tournier@ens-cachan.fr (François Avellan)

1. Introduction

The design and machining process of blade surfaces consists in three steps including Computer-Aided Design (CAD) modeling with CFD optimization of the blade, tool path computation in the Computer-Aided Manufacturing (CAM) software and machining of the part on a machine tool. In this process, the CAD model is the reference model used by any other applications and it usually relies on parametric curves and surfaces with geometrical continuity properties.

From a geometrical point of view, blade modeling is mostly performed by the interpolation of a succession of 2D profiles along the spanwise direction. These 2D profiles are computed whether by the interpolation of a set of sampling points computed by CFD software or directly by the use of parametric curves. The main objectives of the parametric model are to ensure continuity between the curves defining the 2D contour and to reduce the number of geometrical parameters.

However, from a digital mock-up point of view, the degree of polynomial curves and continuity between curves in the parametric model does not matter. Indeed, the geometry of the CAD model is approximated by all the CAX applications based on this model: CFD and Finite Element Analysis (FEA), which generate meshes, visualization using tessellation and even tool path computation, which discretizes surfaces into curves and curves into points as developed hereafter.

During the CAM stage, a set of tool postures (tool position and tool axis orientation) is computed according to a machining strategy [1]. Depending on the design surface, machining is performed in 3 or 5-axis and in flank or end milling. Usual CAM system algorithms for tool path computation rely on the linear format, which is common in the machine tool Numerical Controllers (NC). The surface to be machined is discretized into a set of curves and each curves is discretized into polylines generating geometrical deviations compared to the design. Furthermore, tool paths contain tangency discontinuities which leads to slowdowns during machining and marks on the part due to chip section vari-

31 ations during machining. Post-processors may convert linear tool paths into
 32 polynomial curves. The polynomial trajectory is thus called off-line polynomial
 33 trajectory [2] in opposition to on-line polynomial trajectory that corresponds to
 34 polynomial trajectory calculated in real-time by the NC unit [3]. In both meth-
 35 ods, the polyline is interpolated by polynomial curves such as Bspline curves
 36 according to a geometrical tolerance specified by the user. Consequently, in
 37 the classical design approach, hydraulic optimization of the blade geometry can
 38 provide an optimal design X_d^* , which probably could not be machined without
 39 geometrical deviations.

40

41 To quickly design blades taking into account their machinability, a new
 42 paradigm consists of placing the machining tool path on the heart of the design
 43 process [4]. A continuous polynomial tool path is computed so that the envelop
 44 of the tool movement, not the CAD model, is optimum with respect to the
 45 hydraulic performances. Then, the optimization validates the surface geometry
 46 resulting from a kinematical simulation of the machining, computed with the
 47 Nbuffer method, and CAD model is the 3D representation of the simulation.
 48 Manufacturing should be faster, geometric quality and perceived quality are
 49 improved due to the use of a native polynomial tool path and hydraulic per-
 50 formance should better meet expectations. Therefore, the tool path is modeled
 51 as a native set of Bspline curves and considered as the reference model. CAD
 52 model and CFD/FEA models are then built on these curves through machining
 53 simulation (Table 1).

Table 1: Geometry modeling for the different approaches

Method	CAD	FEA/CFD	CAM	Post-Pro	CNC
Conventional	Curves	Mesh	Points	Points	Points
On line	Curves	Mesh	Points	Points	Curves
Off line	Curves	Mesh	Points	Curves	Curves
Proposed	Mesh	Mesh	Curves	Curves	Curves

54 In the proposed approach, the optimal tool path X_t^* is necessarily machin-
55 able, from a kinematical point of view, but the hydraulic performance will be
56 different from that obtained with the conventional approach X_d^* . Indeed, there
57 is an infinite geometrical solutions to define the blade surface and only one hy-
58 draulic optimal solution. As soon as the parametric models to define the design
59 or the tool path are stated, the range of solutions is reduced as well as the
60 probability of finding the ideal solution. Moreover, as both approaches gener-
61 ate different geometric models, they do not necessarily share the same solution
62 space. Thus, numerical investigations has to be performed to compare hydraulic
63 performances of both approaches.

64 The real challenge would consist to compare both approaches in the case
65 of 5-axis flank milling of 3D blades. Indeed, this process presents a high re-
66 moval material rate a better surface roughness [5]. This process is now widely
67 investigated for the machining of slender complex parts like impellers or turbine
68 blades but it generates undercut and overcut as blades are non developable ruled
69 surfaces or free-form surfaces. Extensive works have been carried out to reduce
70 overcuts and undercuts with cylindrical cutters [6,7,8], conical cutters [9,10] and
71 barrel cutters [11,12]. Still, geometrical deviations are not removed and futher-
72 more, the link between those deviations and the hydraulic performances of the
73 blades has not been investigated.

74 However, full 3D modeling for twisted blades made of non developable sur-
75 faces requires a lot of tests and expensive computational time to setup the
76 process and the evidence of the success of the proposed approach is not guaran-
77 teed. The purpose of this paper is thus to set-up and compare the classical and
78 proposed paradigm to design hydraulic profiles made with developable ruled
79 surfaces. Nevertheless, the use of polynomial curves such as Bezier curves to
80 model the designed profile and the tool path makes this test case relevant. In-
81 deed, the ideal tool path for machining the profile is an offset curve of the profile
82 which equation is known as a rational function. As it is impossible to model the
83 offset curve of a polynomial curve by any polynomial curve, we therefore are
84 dealing with a case which is identical to the machining of non-developable ruled

85 surfaces where X_d^* and X_t^* solutions may be close but will never be identical.

86 The paper is organized as follows: in section 2, a parametric model is pro-
87 posed based on a literature review of 2D profile parameterization. Then, the
88 optimization process is presented in section 3, which includes geometrical mod-
89 eling for both approaches, the CFD simulation and the genetic optimization
90 loop. In section 4, numerical investigations are performed on a single blade in
91 order to compare both approaches.

92 2. 2D blades modeling

93 Two main approaches to design blades are found in the literature: the Shape
94 Inverse Design (SID) and the Global Shape Optimization (GSO) [13,14]. In
95 the SID methods, the designer usually starts from an initial blade geometry
96 and performance and inputs the desired modifications to the performance. SID
97 methods need few iterations to generate a new shape that duplicates the desired
98 surface flow parameters. However, this method requires an initial blade geom-
99 etry computed using a direct approach. In opposition, GSO methods consist
100 in modifying the geometry of the blades until the flow performance is achieved.
101 Methods based on GSO have been developed more recently due to the required
102 computational effort to test and optimize a set of parameters.

103 2D profiles are computed either by the interpolation of a set of sampling
104 points computed by CFD software [15] or directly by the use of parametric
105 curves. Two main variants exist to define the parametric curves [16]. The
106 *Camber-Curve + Thickness* technic and the *Direct Profiling* technic. The camber-
107 curve defines a skeleton and the thickness distribution defines the sides of the
108 profile [17]. This kind of modeling is not well appropriate to define a 2D profile
109 in parametric CAD systems if implicit formulation of the thickness law or of the
110 blade turning angle are used as in [18,19]. A typical example is the definition
111 of NACA 2D profiles, which are imported as sampling points in CAD systems
112 and then re-interpolated.

113 In the method proposed by Koini et al. [20] the camber line is described

114 by a NURBS curve of second degree with three control points (rational Bezier
115 curve). The suction and pressure sides are modeled as Bspline curves defined
116 by control points or interpolation points. The position of these points is defined
117 by a curvilinear abscissa and a normal distance to the camber line.

118 Different works have been published using the direct profile modeling [13,21,24].
119 The main objective is to ensure continuity between the curves defining the 2D
120 contour and to reduce the number of geometrical parameters. Pritchard [21]
121 proposed a geometrical model based on polynomial curves in 1985. The 2D
122 profile consists in five concatenated curves connected in tangency (C^1). The
123 advantage of this model is the reduced number of parameters (9).

124 The model proposed by Pierret et al. [22] consists in three Bezier curves and
125 a circle to design the trailing edge. The connection between the pressure and
126 the suction side at the leading edge ensures a continuous curvature.

127 Anders et al. [23] propose to model the 2D profile by using two Bezier curves
128 of degree 5 for the suction and pressure sides and circles or ellipses to describe
129 the leading and trailing edges. Tangency continuity is ensured at the junction
130 but not curvature continuity. This model leads to 20 parameters.

131 Other methods use only polynomial curves to define the 2D profile. The
132 method proposed by Buche et al. [24] consists in modeling the profile with
133 four polynomial Bezier curves of degree 5 connected in curvature. 16 of the 48
134 required parameters are set by imposing curvature continuity at the junctions.
135 The remaining 32 parameters are translated into engineering parameters and
136 some of them are set to default values leading finally to 19 variable parameters.

137 In [25], Giannakoglou used two Bezier curves of degree 5 to model the pres-
138 sure side and the suction side as well as the leading (LE) and trailing (TE)
139 edges. Both curves shared the same starting and ending points at the LE and
140 TE and ensure tangency continuity at the LE. This parameterization yields to
141 14 parameters.

142 Goel [26] also used two Bezier curves to model the pressure side and the
143 suction side as well as the leading and trailing edges of thick airfoils for high
144 pressure turbines.

Table 2: Number of design parameters

Method	Number of parameters
Pritchard 1985	9
Giannakoglou 2002	14
Goel 2009	14
Pierret et al 1999	15
Dennis et al 1999	17
Buche et al. 2003	19
Anders et al 2008	20
Korakianitis et al. 1993	35
Koini et al. 2009	Unspecified

145 The method proposed by Ghaly et al. [15] consists in approximating an
 146 initial 2D profile by a single Nurbs curve and optimizing the design by moving
 147 the Nurbs control points. The degree of the curve is not specified.

148 In [13], the profiles of suction and pressure surfaces are modeled as two
 149 splines of degree 4. The leading edge is treated separately as a line + thickness
 150 distribution. The construction ensures a third derivative continuity with the
 151 suction and pressure splines.

152 Many combinations of curves are presented to model 2D profiles of turboma-
 153 chines. Among the criteria for discriminating methods, the order of continuity
 154 at the connection between the curves and the number of design parameters is
 155 considered (Table 2). Indeed, fewer parameters lead to shorter computation
 156 time but reduce the variety of possible blade shapes.

157 In the framework of the optimization of hydraulic turbines or impellers, the
 158 method proposed by Koini et al. [20] is adopted to design the blades with a
 159 camber line and a thickness law to define the suction and pressure sides. The
 160 first advantage is the use of a camber line, which shape is directly linked to
 161 hydraulic parameters such as inlet and outlet angles (β_1 and $\beta_{\bar{1}}$). This method
 162 also presents the advantage of an explicit parametric modeling, which is suited
 163 to model the tool path as polynomial curves as well as the design in CAD

164 softwares. The camber line is defined as a Bezier curve $C_L(u)$ (Eq. 1) of degree
 165 2 ($m = 2$) defined by three control points, that is to say 6 parameters.

$$C_L(u) = \sum_{i=0}^m B_{im}(u) \cdot CL_i \text{ with } u \in [0, 1] \quad (1)$$

166 The first control point CL_0 is located on the leading edge and the last one
 167 CL_2 on the trailing edge (Fig. 1). The middle point CL_1 is located at the
 168 intersection between the lines defined with the inlet and outlet angles β_1 and
 169 $\beta_{\bar{1}}$. If a point of the camber line is considered as fixed, only 4 parameters are
 170 required to define it (3 angles and 1 length).

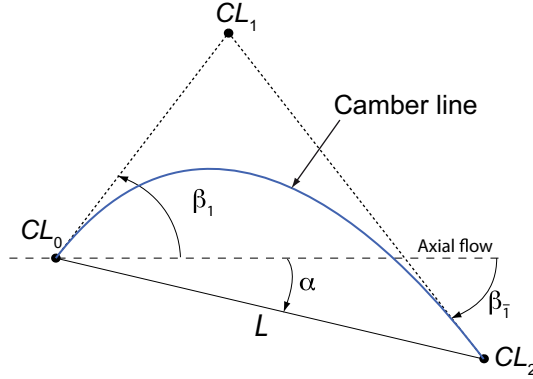


Figure 1: Camber line modeling with Bezier curve

171 Suction and pressure sides are defined by two Bezier curves of degree 4, $S(t)$
 172 and $P(t)$, connected at the leading edge. Each control point S_i or P_i of the
 173 suction and pressure sides (except for $i = 3$) is defined by the abscissa u on the
 174 camber line and the distance d (Fig. 2).

$$S_i = C_L(u_{si}) + d_{si} \cdot \mathbf{n} \quad (2)$$

175

$$P_i = C_L(u_{pi}) + d_{pi} \cdot \mathbf{n} \quad (3)$$

176 The trailing edge, which is defined by the segment S_4P_4 , is sharp to model
 177 real hydraulic blades. The full model is entirely defined by a maximum of 24

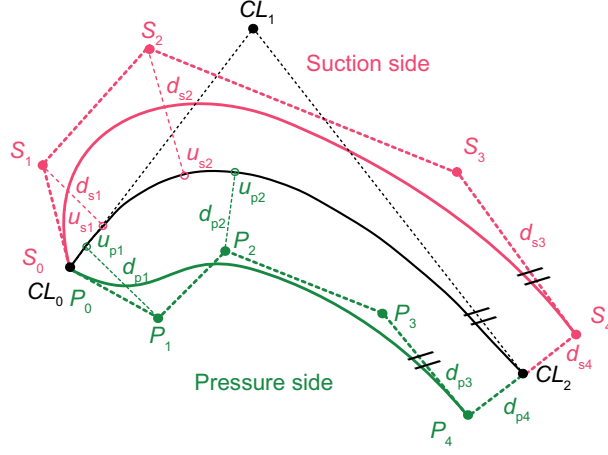


Figure 2: Proposed model

178 parameters. However, the start points $(S_0; P_0)$ and the end points $(S_4; P_4)$ of
 179 both suction and pressure curves are located at the beginning and at the end
 180 of the camber line. This condition ensures a G^0 continuity at the leading edge.
 181 This leads to:

$$u_{s0} = u_{p0} = 0 \quad \text{and} \quad d_{s0} = d_{p0} = 0 \quad (4)$$

182

$$u_{s4} = u_{p4} = 1 \quad (5)$$

183 Furthermore, the points $(S_3; P_3)$ are located on lines parallel to the tangent
 184 to the camber line at CL_2 to respect outlet angle along the profile. They are
 185 defined by two parameters:

$$d_{s3} = S_3S_4 \quad (6)$$

186

$$d_{p3} = P_3P_4 \quad (7)$$

187 Consequently, the maximum number of parameters is equal to 16. Depending
 188 on the continuity at the connection between suction and pressure sides at the

189 leading edge, the number of parameters decreases as mentioned in Table 3. In
 190 the following, the suction side is considered as the anchor curve to define the
 191 pressure side.

Table 3: Total number of parameters vs continuity at the leading edge

Continuity	Suction side	Pressure side	Total
G^0	$[0 \ u_{s1} \ u_{s2} \times 1]$ $[0 \ d_{s1} \ d_{s2} \ d_{s3} \ d_{s4}]$	$[0 \ u_{p1} \ u_{p2} \times 1]$ $[0 \ d_{p1} \ d_{p2} \ d_{p3} \ d_{p4}]$	16
G^1	$[0 \ 0 \ u_{s2} \times 1]$ $[0 \ d_{s1} \ d_{s2} \ d_{s3} \ d_{s4}]$	$[0 \ 0 \ u_{p2} \times 1]$ $[0 \ d_{p1} \ d_{p2} \ d_{p3} \ d_{p4}]$	14
C^1	$[0 \ 0 \ u_{s2} \times 1]$ $[0 \ d_{s1} \ d_{s2} \ d_{s3} \ d_{s4}]$	$[0 \ 0 \ u_{p2} \times 1]$ $[0 \times \ d_{p2} \ d_{p3} \ d_{p4}]$	13
G^2	$[0 \ 0 \ u_{s2} \times 1]$ $[0 \ d_{s1} \ d_{s2} \ d_{s3} \ d_{s4}]$	$[0 \ 0 \ x \times 1]$ $[0 \ d_{p1} \ k_2 \ d_{p3} \ d_{p4}]$	13
C^2	$[0 \ 0 \ u_{s2} \times 1]$ $[0 \ d_{s1} \ d_{s2} \ d_{s3} \ d_{s4}]$	$[0 \ 0 \ x \times 1]$ $[0 \ x \times \ d_{p3} \ d_{p4}]$	11

192 G^1 continuity at the leading edge is achieved if there exists a scalar $k_1 > 0$
 193 so that $\dot{P}(0) = k_1 \cdot \dot{S}(0)$. The first derivative of a Bezier curve $Q(u)$ of degree
 194 m :

$$Q(u) = \sum_{i=0}^m B_{im}(u) \cdot Q_i \text{ with } u \in [0, 1] \quad (8)$$

195 is given for $u = 0$ by:

$$\frac{dQ(0)}{du} = m \cdot (Q_1 - Q_0) \quad (9)$$

196 which leads to the definition of the point P_1

$$P_1 = S_0 + k_1 \cdot (S_0 - S_1) \quad (10)$$

197 with

$$k_1 = \frac{d_{p1}}{d_{s1}} \quad (11)$$

198 If $k_1 = 1$, i.e. $d_{p1} = d_{s1}$, C^1 continuity is achieved.

199

200 G^2 continuity at the leading edge is achieved if there exists a scalar $k_2 > 0$
201 so that $\ddot{P}(0) = k_2 \cdot \ddot{S}(0)$. The second derivative of a Bezier curve $Q(u)$ of degree
202 m for $u = 0$ is given by

$$\frac{d^2Q(0)}{du^2} = m(m-1) \cdot (Q_0 - 2Q_1 + Q_2) \quad (12)$$

203 which leads to the definition of the point P_2

$$P_2 = (1 + 2k_1 + 2k_2) \cdot S_0 - (2k_1 + k_2) \cdot S_1 + k_2 \cdot S_2 \quad (13)$$

204 If $k_1 = 1$ and $k_2 = 1$, C^2 continuity is achieved. Thus, if G^2 or C^2 continuity
205 is prescribed, parameters u_{p2} and d_{p2} are replaced by k_2 .

206 3. Optimization process

207 The proposed method uses an optimization loop containing three separate
208 blocks (Fig. 3): geometrical modeling, CFD simulation and genetic optimiza-
209 tion.

210 3.1. Geometrical modeling

211 The surface profile is modeled as described in the previous paragraph, i.e.
212 using two Bezier curves for suction and pressure sides. In the example depicted
213 in Fig. 4, two Bezier curves of degree 4 are used to model the suction and
214 pressure sides with a curvature continuity C^2 at the leading edge. The trailing
215 edge is sharp and modeled as a straight line. This parameterization leads to 11
216 parameters (Table 4).

217

218 The tool path is modeled with the same parameterization than the design
219 approach, that is to say, by means of two Bezier curves of degree 4 with G^n/C^n
220 continuity at the leading edge (Fig. 5, Table 5). The degree of the Bezier curves
221 has been chosen to be consistent with the maximum degree of polynomial curves

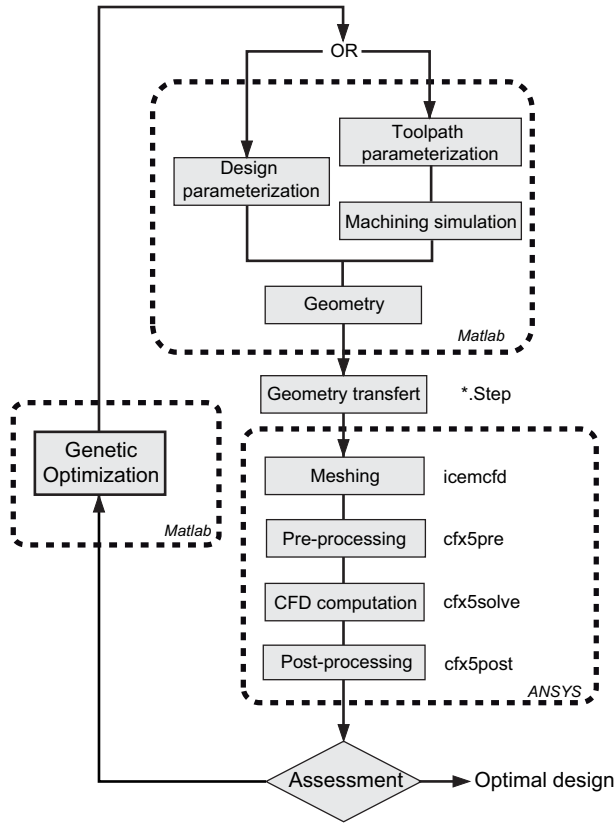


Figure 3: Optimization process

Table 4: C^2 example design parameters

	Camber line	Suction side		Pressure side	
L	0.1 m	u_{s2}	0.3	d_{p3}	0.025 m
α	30°	d_{s1}	0.005 m	d_{p4}	0.002 m
β_1	0°	d_{s2}	0.015 m		
$\beta_{\bar{1}}$	60°	d_{s3}	0.045 m		
		d_{s4}	0.002 m		

222 a numerical controller could interpolate, which is equal to 5 for a Siemens 840D
 223 [27]. In this way, the proposed design process ensures a full polynomial model
 224 from design to manufacturing without any geometric approximation.

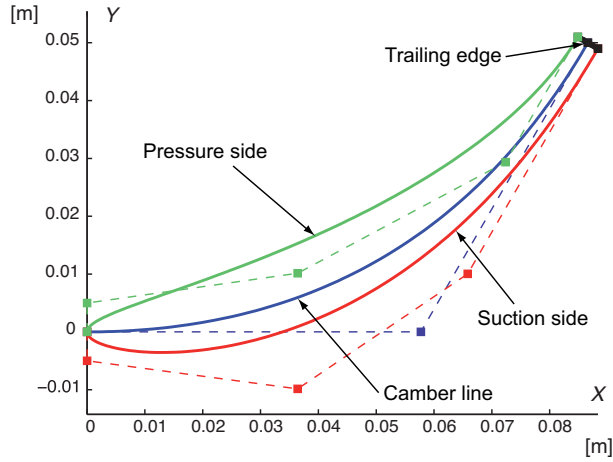


Figure 4: C^2 design example

225 The first control point of both curves at the leading edge is the offset of the
 226 origin point of the camber line CL_0 along its tangent vector with a magnitude
 227 equal to the tool radius.

$$S_0 = P_0 = CL_0 + R \cdot \mathbf{t} \quad (14)$$

228 The last control point of both curves at the trailing edge is the offset of the
 229 last point of the camber line CL_2 along its normal vector with a magnitude
 230 greater or equal to the tool radius.

$$S_4 = CL_2 + (R + d_{s4}) \cdot \mathbf{n} \quad (15)$$

231

$$P_4 = CL_2 - (R + d_{p4}) \cdot \mathbf{n} \quad (16)$$

232 The points describing the blade surface are generated through a kinematical
 233 machining simulation. They are defined as points of the envelope surface of the
 234 tool movement computed by a N-buffer algorithm [28] (Fig. 6). This consists
 235 in computing intersections between the straight lines of the N-buffer with the
 236 cylindrical tool. Those points are then used to build the mesh during CFD
 237 simulation.

Table 5: G^1 example tool path parameters

	Camber line		Suction side		Pressure side
L	0.1 m	u_{s2}	0.2	u_{p2}	0.25
α	30°	d_{s1}	0.013 m	d_{p1}	0.012 m
β_1	0°	d_{s2}	0.019 m	d_{p2}	0.014 m
$\beta_{\bar{1}}$	60°	d_{s3}	0.020 m	d_{p3}	0.025 m
		d_{s4}	0.007 m	d_{p4}	0.007 m

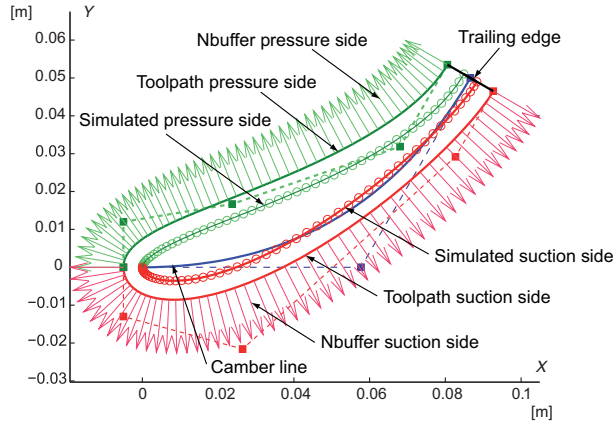


Figure 5: G^1 tool path example

238 *3.2. CFD simulation*

239 The quality of the mesh is an important issue to ensure the quality of the
 240 results. In order to obtain accurate results and a robust automatic mesh gener-
 241 ation during the optimization process, a hybrid (structured/unstructured) mesh
 242 is used as shown in Fig. 7.

243 The separation between the two mesh types is performed by the convex
 244 envelope of a profile's offset. This offset is taken with a magnitude equal to 10
 245 percent of the chord (L) for the suction and pressure sides and 20 percent for
 246 the trailing edge. The convex envelope is used to ensure the robustness of the
 247 automatic mesh generation in case of a high curvature blade.

248 The structured mesh is located between the profile and the offset (O-mesh).

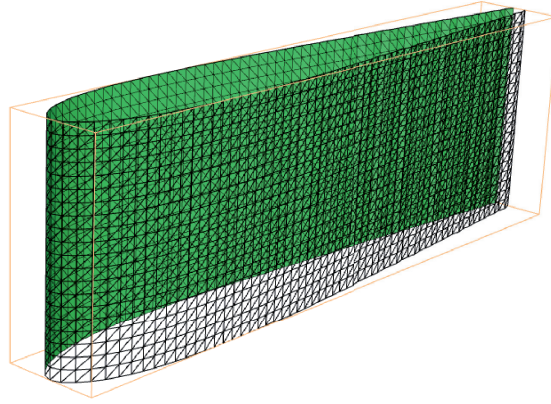


Figure 6: Blade generated with N-buffer simulation

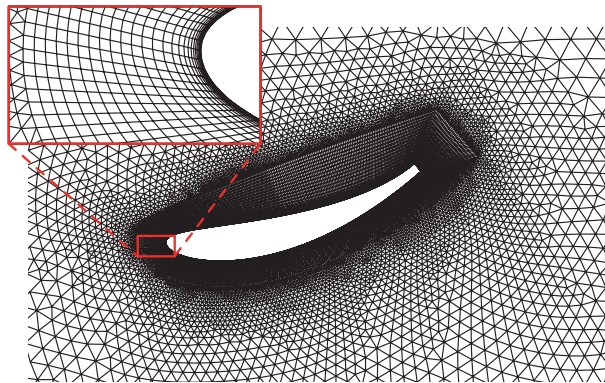


Figure 7: Hybrid mesh

249 In this way, the boundary layer effects are well captured due to the better
250 accuracy of this kind of mesh. The unstructured mesh is located between the
251 offset and the boundaries of the fluid domain. Therefore, topological constraints
252 do not depend on the relative position of the profile regarding to the boundaries.

253 The mesh generation is done during the optimization within ANSYS ICEM
254 through a replay script-file written in Tcl/Tk language. The total number of
255 mesh nodes is approximately 100'000 due to the different profiles shapes.

256 The quality of the mesh is checked for the optimal blades at each iteration.

257 The quality criterions for a mesh cell are a minimum angle greater than 15 de-
 258 grees and a relative Jacobian determinant greater than 0.4 [29].

259

260 In the present study, the water is assumed as incompressible at constant
 261 temperature. The motion of the water is governed by the Reynolds Averaged
 262 Navier Stokes (RANS) equations (17) and (18), where p is the static pressure,
 263 ν is the kinematic viscosity and $X_i = [X, Y, Z]$ the components of the Cartesian
 264 coordinate system. In these equations, the velocity and pressure are split into
 265 a mean value and a fluctuating part (19). The Reynolds stresses term defined
 266 as $\overline{\rho C'_i C'_j}$ is modelled by the Shear Stress Transport (SST) turbulence model,
 267 which is described by Menter et al. [30].

$$\frac{\partial \overline{C}_i}{\partial X_i} = 0 \quad \text{and} \quad \frac{\partial C'_i}{\partial X_i} = 0 \quad (17)$$

268

$$\frac{\partial \overline{C}_i}{\partial t} + \overline{C}_j \frac{\partial \overline{C}_i}{\partial X_j} = -\frac{1}{\rho} \frac{\partial \overline{p}}{\partial X_i} + \nu \frac{\partial^2 \overline{C}_i}{\partial X_j^2} - \frac{\partial \overline{C'_i C'_j}}{\partial X_j}. \quad (18)$$

269

$$C_i = \overline{C}_i + C'_i \quad \text{and} \quad p = \overline{p} + p' \quad (19)$$

270 The dimensions of the computational domain as well as the different bound-
 271 ary conditions are illustrated in Fig. 8.

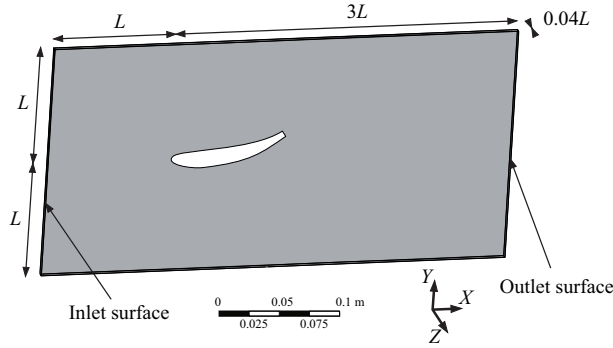


Figure 8: Computational domain

272 At the inlet surface, a uniform reference velocity C_0 is applied and decom-
 273 posed as follow: $C_X = 10 \text{ m s}^{-1}$, $C_Y = 0 \text{ m s}^{-1}$ and $C_Z = 0 \text{ m s}^{-1}$. Moreover,

274 a turbulent intensity of 5% percent is chosen for the inlet, which corresponds
275 to a medium turbulent intensity. On the outlet surface, a zero average static
276 pressure is imposed. The suction side, pressure side and trailing edge surfaces
277 of the blade are set as no-slip smooth walls. Therefore, the velocity on these
278 surfaces is imposed equal to zero. On the top, bottom and sides surfaces a
279 symmetric boundary conditions is applied [31].

280 In order to improve the convergence of the computation, the initial conditions
281 for the velocity and pressure are taken from the result of a simulation, which
282 corresponds to the middle of the parameters range (Table 6).

283 The software used for the different numerical flow simulation is the com-
284 mercial code ANSYS-CFX Release 12.1. The geometry of the computational
285 domain is imported from ANSYS-ICEM. Then, the selected numerical setup
286 for the case study is applied in ANSYS-CFX-Pre. Afterwards, the numerical
287 simulation is performed by ANSYS-CFX-Solver.

288 This solver uses a finite volume discretization of the equations. Conse-
289 quently, the continuous value of velocity and pressure of the flow field are dis-
290 cretized on each mesh node in order to solve implicitly a system of algebraic
291 equations. The stop criterion for the computation is a maximum residual of
292 $5 \cdot 10^{-6}$ for each unknown variable or a maximum number of 300 iterations.

293 The results are analyzed with ANSYS-CFX-Post where the interesting values
294 for the optimization process are extracted. In the present study, the extracted
295 values are: the drag force F_X , the lift force F_Y , the maximum velocity value in
296 the computational domain C_{max} and the non dimensional wall distance y^+ .

297 The maximum velocity value in the computational domain is used to eval-
298 uate the specific energy losses in the computational domain. Indeed, as these
299 losses are proportional to $\frac{C^2}{2}$, the minimization of C_{max} corresponds to the
300 minimization of the losses.

301

302 The non dimensional wall distance value y^+ represents the ability of the mesh
303 to take into account the physic of the flow (Eq. 20). This value is proportional
304 to the height of the mesh elements in contact with the blade and to the friction

305 velocity u_τ . After each computation, a maximum y^+ value below 20 is checked
 306 on the profile to simulate the boundary layer behavior and verify the mesh
 307 quality.

$$y^+ = \frac{u_\tau \cdot y}{\nu} \quad \text{with} \quad u_\tau = \sqrt{\frac{\tau_p}{\rho}} \quad (20)$$

308 3.3. Genetic optimization

309 The genetic algorithms are based on the principles of natural genetics and
 310 evolution. At each step of the optimization process, the algorithm computes the
 311 objectives for each individual. Then, the population is sorted and scaled in order
 312 to select the individuals, which will be used to produce the next population. This
 313 population is either produced by the mutation of a selected individual (18%)
 314 or by the crossover of two selected individuals (80%) and with the two best
 315 individuals from the previous iteration (2%) [33].

316 In the present analysis, the multi-objective optimization process is performed
 317 with the global optimization toolbox from Matlab. The size of this population
 318 is set to 100 different profiles and the maximum number of iterations is limited
 319 to 50, which leads to approximately 5'000 computations per optimization run.

320 The design and tool path parameters are limited by the parameters range
 321 given in Table 6. Moreover, linear constraints are applied inside the optimization
 322 process in order to produce only feasible profile shape (Eq. 21).

$$\beta_1 \leq \alpha \quad \text{and} \quad \alpha \leq \beta_{\bar{1}} \quad (21)$$

323 In the case of tool path optimization, the curvature radius R_κ of both suction
 324 and pressure sides has to be greater than the tool radius R to prevent the
 325 generation of a loop in the offset profile (Eq. 22).

$$R_\kappa = \frac{\|\ddot{\mathbf{Q}}(u)\|^3}{\|\dot{\mathbf{Q}}(u) \times \ddot{\mathbf{Q}}(u)\|} \quad \text{and} \quad R_\kappa \geq R \quad (22)$$

326 As the purpose of this paper is to compare the design and tool path ap-
 327 proaches in order to generate a blade, only two objectives are arbitrarily chosen
 328 for the present study: maximize F_Y and minimize C_{max} .

329

330 To decrease the time of the optimization process, the genetic algorithm is
 331 used in parallel. Therefore, the simulations of the population are sent to a
 332 computational grid to compute several individuals in the same time.

333 4. Numerical investigations

334 Numerical investigations have been conducted for eight different cases, gath-
 335 ering the two methods and four types of continuity at the leading edge between
 336 suction and pressure sides. The range of the geometrical parameters is given in
 337 Table 6.

Table 6: Range of parameters

Parameter	Min	Max	Design	tool path
α	-5°	25°	x	x
β_1	-20°	30°	x	x
β_T	0°	50°	x	x
u_{s2}	0.01	0.35	x	x
d_{s1}	0.005 m	0.008 m	x	o
d_{s1}	0.008 m	0.011 m	o	x
d_{s2}	0.005 m	0.015 m	x	x
d_{s3}	0.02 m	0.05 m	x	x
d_{s4}	0.002 m	0.002 m	x	x
u_{p2}	0.01	0.35	x	x
d_{p1}	0.005 m	0.008 m	x	o
d_{p1}	0.008 m	0.011 m	o	x
d_{p2}	0.005 m	0.015 m	x	x
d_{p3}	0.02 m	0.05 m	x	x
d_{p4}	0.002 m	0.002 m	x	x
R	0.005 m	0.005 m	o	x

338 For each case study, ten Intel Xeon CPU at 3.00 GHz with eight cores and
 339 8 GB of memory are used in parallel during the genetic optimization and each
 340 numerical simulation is carried out on four cores. The mean computing time
 341 for the simulation of an individual is ten minutes, which leads to an averaged

342 time of one hour per iteration.

343 The objectives are maximization of the lift F_Y and minimization of the
344 maximal velocity C_{max} . The resulting values for the eight cases are gathered
345 in Table 7. Moreover, lift coefficients C_L and pressure coefficient $C_{p,min}$ have
346 been calculated to non-dimensionalize the results.

$$C_L = \frac{F_Y}{\rho \cdot \frac{C_0^2}{2} \cdot 0.04L^2} \quad \text{and} \quad C_{p,min} = 1 - \frac{C_{max}^2}{C_0^2} \quad (23)$$

347 The magnitude of lift F_Y and maximum velocity C_{max} are approximately
348 the same for both methods and for the different levels of continuities (Table
349 7). However, in the C^2 case, the maximum lift is lower by about 15% for both
350 design and tool path approaches. This is because the C^2 continuity constraint
351 at the leading edge blocks the first three control points of the pressure side
352 (P_0, P_1, P_2), thereby reducing the degrees of freedom for the generation of the
353 blades.

354 The lift difference between the two methods is always lower than 4%. This
355 is not significant because it has the same order of magnitude as the amplitude
356 of lift fluctuation (± 5 N). Indeed, the high curvature profiles generate vortices
357 shedding, which induces a fluctuating lift value during the computation despite
358 the use of a steady solver. Moreover, the differences in the optimization results
359 are likely well within the errors introduced by the RANS model for the complex
360 flows over such blades.

361 The maximal velocity C_{max} (or the pressure coefficient $C_{p,min}$) is always
362 greater for the tool path method because the curvature radius at the leading
363 edge is imposed by the choice of parameters d_{s1} and d_{s2} . Indeed, if these param-
364 eters are too small, the radius of curvature of the generated tool path is lower
365 than the tool radius and the N-buffer simulation is not allowed. The choice of
366 the range of these parameters (Table 6) may have been too conservative result-
367 ing in more flattened edges, generating slightly higher speed along the profile.

368

369 Since there are two different objectives in the optimization, the Pareto fronts

Table 7: Optimisation results

Case	Max $ F_Y $ [N]	Max C_L [-]	Min C_{max} [m s ⁻¹]	Min $ C_{p,min} $ [-]
G^1 Design	84.14	4.20	12.15	0.48
G^1 Tool path	88.16	4.41	12.25	0.50
C^1 Design	87.00	4.35	11.66	0.36
C^1 Tool path	84.30	4.21	12.08	0.46
G^2 Design	88.00	4.40	11.73	0.38
G^2 Tool path	84.74	4.23	12.49	0.56
C^2 Design	78.02	3.90	11.73	0.37
C^2 Tool path	76.40	3.82	12.80	0.64

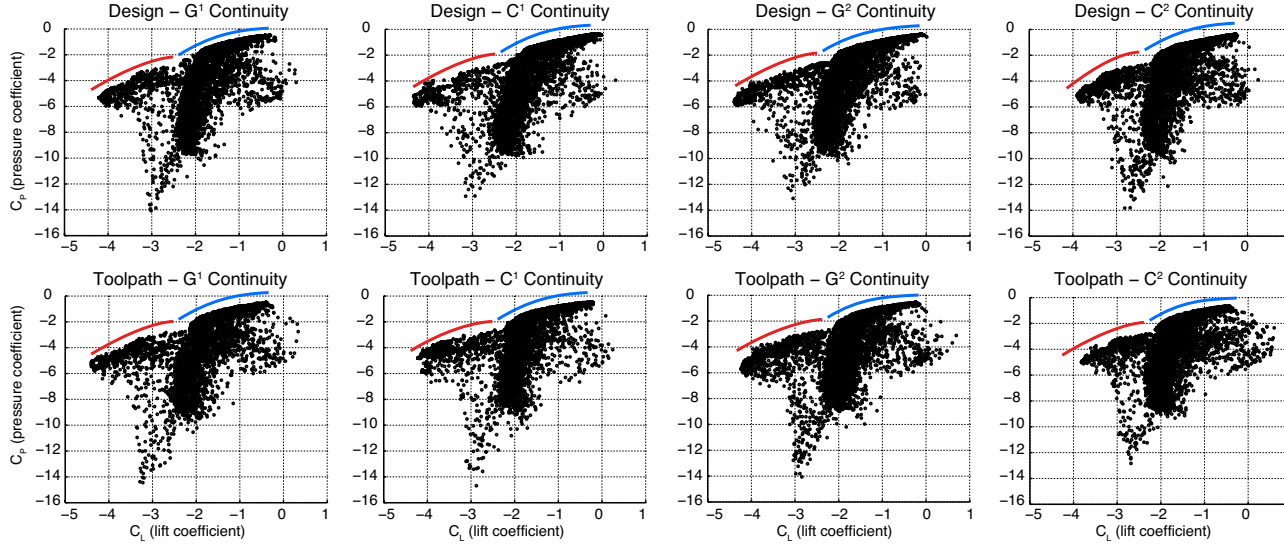


Figure 9: Pareto fronts

370 for the eight cases have been plotted on Fig. 9. It shows that the Pareto fronts
 371 resulting from the optimization of the two criteria C_L and $C_{p,min}$ have the
 372 same shape and are divided into two zones.

373 The Pareto fronts for the G^1 case with design and tool path approaches
374 have been illustrated in Fig. 10 and Fig. 11. Six points on each Pareto front
375 have been chosen and their hydraulic properties have been highlighted. These
376 points are as near as possible for both cases but can't be exactly identical.
377 The geometry of the blades corresponding to the selected hydraulic properties
378 are presented respectively in Fig. 12 and Fig. 13. Results show that there
379 are two different families of blade geometry, which depends strongly on the
380 angles that define the camber line (α , β_1 and $\beta_{\bar{1}}$). The geometries created by
381 the conventional approach and the proposed one are similar. Slender blades
382 generate slow velocity profiles whereas curved blades generate high lift values
383 which is coherent with the theory. Both approaches lead to this behavior, which
384 proves that the proposed approach is consistent.

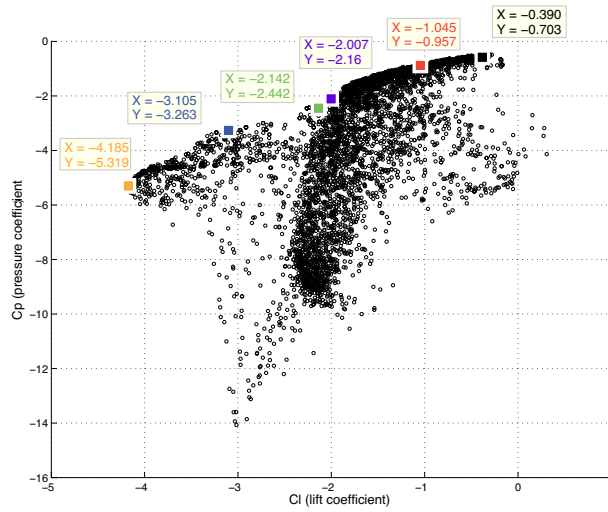


Figure 10: Pareto front ; design G^1 continuity

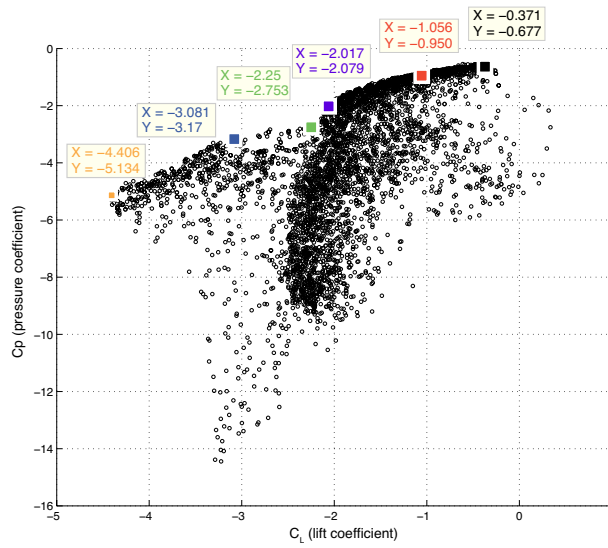


Figure 11: Pareto front ; tool path G^1 continuity

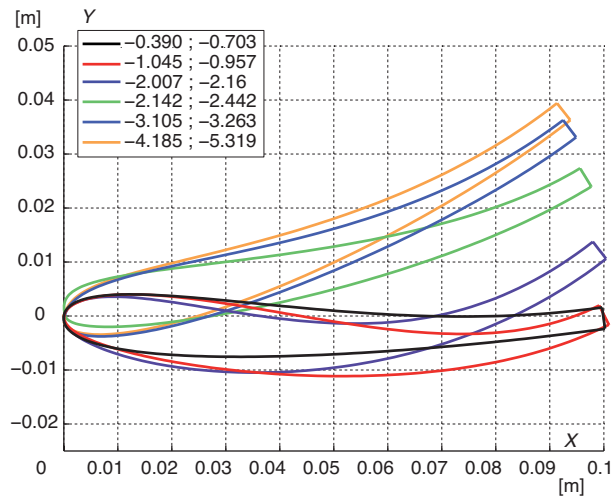


Figure 12: Geometries on Pareto front ; design G^1 continuity

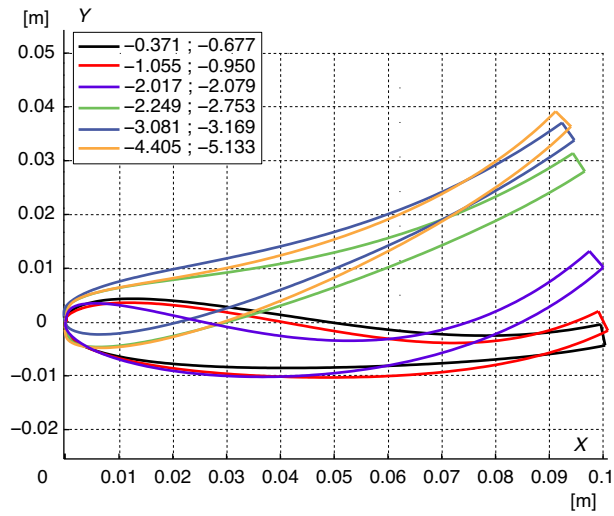


Figure 13: Geometries on Pareto front ; tool path G^1 continuity

385 5. Conclusions

386 In this paper, a different approach to design hydrodynamic profiles has been
387 developed. This approach is based on the definition of a tool path such that
388 the envelope of the movement of the tool optimizes one or more hydrodynamic
389 criteria. A unified parametric model to design the blades for both approaches
390 (design and tool path) was proposed as well as a robust automatic meshing
391 strategy to mesh the fluid domain based on different blade geometries.

392 Overall, the results show that the proposed approach can generate geome-
393 tries whose performances are comparable to the ones obtained by the classical
394 approach. The advantage is that these performances are not degraded because
395 the same polynomial curves would be used from the design stage to the ma-
396 chining stage without modifications in the post-processor or in the NC unit.
397 Polynomial format ensures the smoothness of the trajectory, which is one of
398 the parameters required to provide a good surface finish. To enhance the op-
399 timization, machining phenomena such as dynamical behavior of the machine
400 tool could be introduced in the machining simulation.

401 The method was validated on a 2D example. The next step is the design and
402 manufacture of impellers, usually designed with non-developable ruled surfaces,
403 which are impossible to machine in 5-axis flank milling without geometrical
404 deviations. However, the large number of parameters to control the geometry
405 of such complex blades suggests to use faster optimization technics than genetic
406 algorithms.

407 **Nomenclature**

Geometric parameters

m	Degree of the curve [-]
u	Curvilinear abscissa [-]
$B_{im}(u)$	Bernstein polynomial i [-]
$Q(u)$	Bezier curve [-]
Q_i	Control point i [-]
$\beta_1, \beta_{\bar{1}}$	Inlet, outlet angle [°]
L	Chord length [m]
α	Chord angle [°]
$C_L(u)$	Camber line function [m]
CL_i	Camber line control point i [m]
\mathbf{n}	Vector normal to camber line [m]
\mathbf{t}	Vector tangent to camber line [m]
$S(t), P(t)$	Suction, pressure side function [m]
S_i, P_i	Control point i [m]
u_{si}, u_{pi}	Control points abscissa i [-]
d_{si}, d_{pi}	Control points distance i [m]
G^n, C^n	Continuity degree n [-]
k_n	G^n/C^n continuity parameter [-]
R	Tool radius [m]
R_κ	Curvature radius [m]
X_d^*, X_t^*	Optimal design, optimal tool path [-]

408

CFD parameters

X, Y, Z	Cartesian component [m]
X_i	Cartesian component i [m]
C	Absolut velocity [m s^{-1}]
C_i	Absolut velocity component i [m s^{-1}]
C_0	Reference velocity at inlet [m s^{-1}]
p	Static pressure [Pa]
ρ	Density [kg m^{-3}]
ν	Kinematic viscosity [$\text{m}^2 \text{s}^{-1}$]
F_X, F_Y	drag, lift force [N]
y^+	Wall distance [–]
τ_p	Wall shear stress [Pa]
C_L	Lift coefficient [–]
C_p	Pressure coefficient [–]

409

Abbreviations

CAD	Computer Aided Design
CAM	Computer Aided Manufacturing
CFD	Computer Fluids Dynamics
FEA	Finite Element Analysis
GSO	Global Shape Optimization
LE	Leading Edge
NS	Navier Stokes
NC	Numerical Controllers
RANS	Reynolds Averaged Navier Stokes
SID	Shape Inverse Design
SST	Shear Stress Transport
TE	Trailing Edge

410

411 **References**

- 412 [1] B.K. Choi , R.B. Jerard. Sculptured surface machining, theory and appli-
413 cations. Dordrecht: Kluwer Academic Publishers, 1998.
- 414 [2] C. Lartigue, F. Thiebaut, T. Maekawa, CNC tool path in terms of B-spline
415 curves, *Computer-Aided Design* 2001;33:307-319.
- 416 [3] Cheng, M.-Y., Tsai, M.-C., Kuo, J.-C., Real-time Nurbs command genera-
417 tors for CNC servo-controllers, *International Journal of Machine Tools and*
418 *Manufacture* 2002;42(7):801-813.
- 419 [4] E. Duc, C. Lartigue, C. Tournier and P. Bourdet, A new concept for the
420 design and the manufacturing of free-form surfaces: the machining surface.
421 *CIRP Annals - Manufacturing Technology* 1999;48(1):103-106.
- 422 [5] H. Tonshoff, N. Rackow, Optimal tool positioning for five-axis flank milling
423 of arbitrary shaped surfaces, *Annals of the German Academic Society for*
424 *Production Engineering (WGP)* 2000;7(1): 57-60.
- 425 [6] C. Menzel, S. Bedi, S. Mann, Triple tangent flank milling of ruled surfaces,
426 *Computer-Aided Design* 2004;36(3):389-296.
- 427 [7] J. Senatore, F. Monies, J.-M. Redonnet, W. Rubio, Analysis of im-
428 proved positioning in five-axis ruled surface milling using envelope surface,
429 *Computer-Aided Design* 2005;37(10):989-998.
- 430 [8] P.-Y. Pechard, C. Tournier, C. Lartigue, and J.-P. Lugarini. Geometrical
431 deviations versus smoothness in 5-axis flank milling. *International Journal*
432 *of Machine Tools and Manufacture* 2009;49(6):454-461.
- 433 [9] C. Lartigue, E. Duc, A. Affouard, Tool path deformation in 5-axis milling
434 using envelope surface, *Computer-Aided Design* 2003;35(4):375-382.
- 435 [10] L. Zhu, G. Zheng, H. Ding, and Y. Xiong. Global optimization of tool path
436 for five-axis flank milling with a conical cutter. *Computer-Aided Design*
437 2010;42(10):903-910.

- 438 [11] J. Chaves-Jacob, G. Poulachon, and E. Duc. New approach to 5-axis
439 flank milling of free-form surfaces: Computation of adapted tool shape.
440 *Computer-Aided Design* 2009;41(12):918-929.
- 441 [12] H. Gong, F. Z. Fang, X. T. Hu, L.-X. Cao, and J. Liu. Optimization of
442 tool positions locally based on the bcelp for 5-axis machining of free-form
443 surfaces. *Computer-Aided Design* 2010;42(6):558-570.
- 444 [13] T. Korakianitis and G. Pantazopoulos. Improved turbine-blade design tech-
445 niques using 4th-order parametric-spline segments. *Computer-Aided De-
446 sign* 1993;25(5):289-299.
- 447 [14] B. Dennis, G. Dulikravich, and Z.-X. Han. Constrained shape optimization
448 of airfoil cascades using a navier-stokes solver and a genetic/sqp algorithm.
449 In *ASME, International Gas Turbine and Aeroengine. Congress and Exhi-
450 bition, Indianapolis, USA, 1999.*
- 451 [15] W. S. Ghaly and T. T. Mengistu. Optimal geometric representation of
452 turbomachinery cascades using nurbs. *Inverse Problems in Science and En-
453 gineering* 2003;11(5):359-373.
- 454 [16] L. Ferrando, J.-L. Kueny, F. Avellan, C. Pedretti, and L. Thomas. Surface
455 parameterization of a francis runner turbine for optimum design. In *22nd
456 IAHR Symposium on Hydraulic Machinery and Systems, 2004.*
- 457 [17] L. Ferro, L. Gato, and A. Falcao. Design and experimental validation of
458 the inlet guide vane system of a mini hydraulic bulb-turbine. *Renewable
459 Energy* 2010;35(9):1920-1928.
- 460 [18] I. Abbott and A. Doenhoff. *Theory of wing sections: including a summary
461 of airfoil data.* Dover books on physics and chemistry. Dover Publications,
462 1959.
- 463 [19] D. Bonaiuti, A. Arnone, M. Ermini, and L. Baldassarre. Analysis and op-
464 timization of transonic centrifugal compressor impellers using the design of
465 experiments technique. *Journal of Turbomachinery* 2006;128(4):786-797.

- 466 [20] G. N. Koini, S. S. Sarakinos, and I. K. Nikolos. A software tool for para-
467 metric design of turbomachinery blades. *Advances in Engineering Software*
468 2009;40(1):41–51, 1.
- 469 [21] L. Pritchard. An eleven parameter axial turbine airfoil geometry model. In
470 *ASME 1985;85-GT-219*.
- 471 [22] S. Pierret and R. A. Van den Braembussche. Turbomachinery blade de-
472 sign using a navier-stokes solver and artificial neural network. *Journal of*
473 *Turbomachinery* 1999;121(2):326–332.
- 474 [23] J. M. Anders, J. Haarmeyer, and H. Heukenkamp. A parametric blade
475 design system (part i + ii) Von Karman Institut lecture serie1, 2008.
- 476 [24] D. Buche, G. Guidati, and P. Stoll. Automated design optimization of
477 compressor blades for stationary, large-scale turbomachinery. *ASME Con-*
478 *ference Proceedings* 2003;(36894):1249-1257.
- 479 [25] K. C. Giannakoglou. Design of optimal aerodynamic shapes using stochas-
480 tic optimization methods and computational intelligence. *Progress in*
481 *Aerospace Sciences* 2002;38(1):43-76.
- 482 [26] S. Goel. Turbine airfoil optimization using quasi-3d analysis codes. *Inter-*
483 *national Journal of Aerospace Engineering*, 2009.
- 484 [27] Siemens. www.automation.siemens.com/doconweb,
485 Sinumerik 840D/840Di/810D user, Programming Manual Job planning, 2010.
- 486 [28] R. Jerard, R. Drysdale, K. Hauck, B. Schaudt, and J. Magewick. Meth-
487 ods for detecting errors in numerically controlled machining of sculptured
488 surfaces. *IEEE Computer Graphics and Applications* 1989;9(1):26–39.
- 489 [29] ANSYS ICEM CFD 12.1. Help Manual, 2009.
- 490 [30] F. R. Menter, M. Kuntz, R. Langtry. Ten years of industrial experience
491 with the SST turbulence model. Begell House Inc, 2003.

- 492 [31] ANSYS CFX-Solver 12.1. Theory Guide, 2009.
- 493 [32] I. L. Ryhming. Dynamique des fluides. 2nd Edition, Presses Polytechniques
494 et Universitaires Romandes, 2004
- 495 [33] U. Maulik, S. Bandyopadhyay, A. Mukhopadhyay. Multiobjective genetic
496 algorithms for clustering. Springer, 2011